Simulation of the regional climatic impact of Amazon deforestation

J. Lean & D. A. Warrilow*

Dynamical Climatology Branch, Meteorological Office, Bracknell, Berkshire RG12 2SZ, UK
* Present Address: Global Atmosphere Division, Department of Environment, London SW1P 3PY, UK

THE Amazon basin contains about half of Earth's Tropical forest[1]. Population pressure and subsequent demands for crop production, timber and firewood have led to rapid deforestation. Quantitative estimates of the rate of deforestation from analysis of Landsat observations indicate that rates are increasing exponentially in many regions[2,3], but the precise figures are not known[4]. Removal of the protection provided by natural cover can lead to soil erosion, disturbance of the ecosystem and reduction in species diversity[5]. Here we report results from a three-year simulation, using a general circulation model, in which we replace Amazon tropical forest and savannah with pasture. The simulated local climate response was dominated by a weakened hydrological cycle, with less precipitation and evaporation and an increase in surface temperature. The reductions in precipitation and evaporation were mostly caused by changes in surface roughness and albedo: decreased roughness dominated the reduction in evaporation (and the increase in temperature), whereas the increased albedo was the main cause of a decrease in the moisture flux convergence (measured as the difference between precipitation and evaporation) contributing to the decrease in precipitation.

Within the Amazon basin, it is estimated that 50% of the rainfall is derived from local evaporation[6], and it has been suggested that a significant reduction in tropical forest might reduce evaporation and rainfall[7]. Recently, various studies concerning the impact of surface changes on climate have been carried out using three-dimensional atmospheric global climate models (AGCMs). A review of tropical deforestation experiments[8] shows that substantial differences exist between the schemes for representing physical processes (parameterizations) and between methods used to simulate land transformations in AGCMs. As a result AGCMs have not presented a uniform picture of the potential effects of deforestation on climate. The use of rather simple land surface schemes and the lack of grid-scale data with which to calibrate the models make the applicability of the results uncertain. Some common points, however, have emerged from these simulations. First, albedo, roughness and surface hydrology are the most important variables for the representation of land transformation. Second, results are sensitive to the parameterization processes in the model, to the choice of vegetation and soil parameters and the soil-moisture field as input data, and the climatology of the AGCM. Over the past few years more realistic land surface parameterizations have been included in various AGCMs including that of the UK Meteorological Office.

Here we describe experiments that were carried out using the $2\frac{1}{2}° \times 3\frac{3}{4}°$ resolution AGCM described in ref. 9, but including a more complex representation of interactive cloud processes[10]. The land surface parameterization (D.A.W., A. B. Sangster and A. Slingo, unpublished results) includes a four-layer soil temperature scheme. Interception of precipitation by a vegetation canopy is represented, allowing zero resistance to re-evaporation and potentially a more realistic partitioning of energy between latent- and sensible-heat fluxes. The hydrological scheme diagnoses surface runoff from the excess of rainfall over infiltration capacity (accounting for the spatial variability of rainfall statistically), and subsurface runoff from the gravitational drainage of soil moisture[11]. Geographical variation of land surface and soil types is based on the work of Wilson and Henderson-Sellers[12]. Their original $1° \times 1°$-resolution primary- and secondary-vegetation datasets were used to create spatially varying datasets of 17 soil and vegetation parameters which were interpolated onto our $2\frac{1}{2}° \times 3\frac{3}{4}°$ model grid[13].

We ran three-year control and deforestation experiments, starting at the end of June. All grid boxes in South America north of 30° S defined as either tropical forest or savannah on the $1° \times 1°$ grid were replaced by tropical pasture. Soil characteristics except surface infiltration capacity, were left unaltered. We give the results for an area in the southern part of Amazonia where the largest change in land surface characteristics occurred (see Fig. 1).

We compare the control simulation with observation in Fig. 1 and Table 1. The model simulates accurately the spatial distribution of rainfall for both the Southern Hemisphere winter and summer, although the dry areas are more extensive in winter over the southern Amazon and rainfall is slightly excessive in summer over the basin. Looking particularly at the region concerned, Fig. 2*a* shows this slight amplification of the seasonal cycle in the control rainfall simulation. The annual mean values of other variables, compared in Table 1, show that the control simulation is quite realisitc. We note that it is extremely difficult to obtain accurate estimates of such quantities because observations are too sparse to provide grid-square means. Runoff is

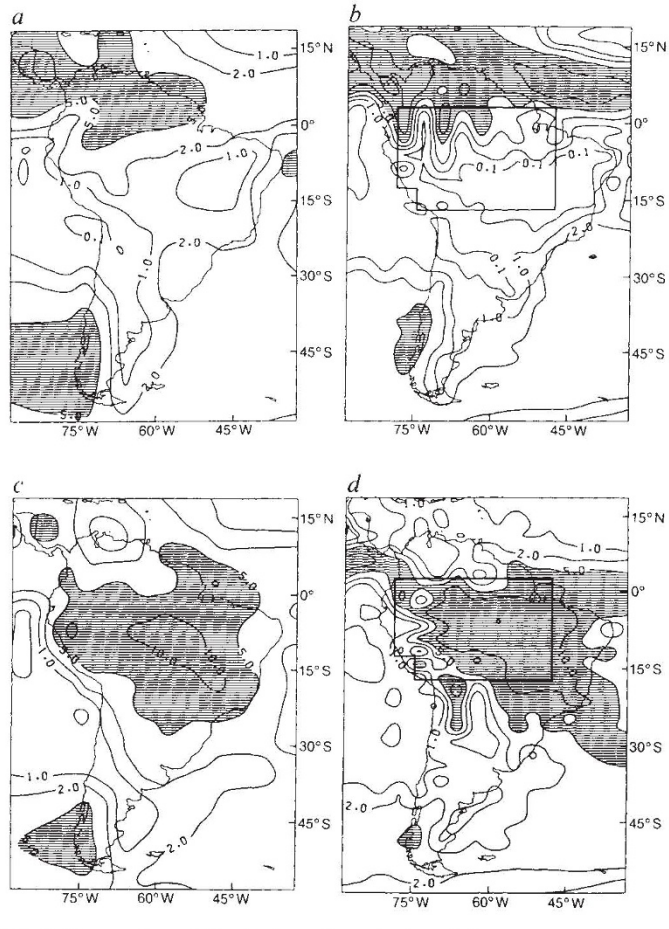

FIG. 1 The section within the box shown in *b* and *d* represents the area selected for averaging purposes for all results quoted and represents the area having the largest change in land surface characteristics in the southern region north of 30° S. *a*, Observed[21] precipitation pattern over South America for the Southern Hemisphere winter (June, July and August). Contours are at 0.1, 1.0, 2.0, 5.0, 10.0 and 20.0 mm d^{-1} and shading is above 5 mm d^{-1}. *b*, Simulated precipitation pattern of the control experiment over South America for the Southern Hemisphere winter averaged over three years. *c*, As for *a* but for the Southern Hemisphere summer (December, January and February). *d*, As for *b* but for the Southern Hemisphere summer.

TABLE 1 Summary of surface variables

Surface Variable	C*	D†	O‡
Evaporation (mm d^{-1})	3.12	2.27 (−27.2%)	3.34 (ref. 21)
Precipitation (mm d^{-1})	6.60	5.26 (−20.3%)	5.26 (ref. 22)
Soil moisture (cm)	16.13	6.66 (−58.7%)	
Runoff (mm d^{-1})	3.40	3.0 (−11.9%)	2.76 (ref. 23)
Net radiation (W m^{-2})	147.3	126.0 (−14.5%)	
Temperature (°C)	23.6	26.0 (+2.4 °C)	24.0 (ref. 24)
Sensible heat (W m^{-2})	57.2	60.2 (+5.2%)	
Bowen Ratio	0.85	1.5 (+76.5%)	

* Control simulation, averaged over three years.
† Deforested simulation, averaged over three years.
‡ Observations.

only quoted for a particular basin and is not strictly comparable to that from the region shown. Evaporation is based on only a few direct observations and empirical calculations.

Comparison of surface quantities for a single model grid square with data[14] for a site in central Amazonia indicates that modelled total evaporation differs by 15% from the observed, and that the modelled canopy evaporation is 71% compared with the observed 25% of total evaporation. Overestimation of canopy evaporation is probably present in other land surface schemes and this may be due[15] to the extension of a single-point description of the rainfall interception process to the grid-scale area in a region where convective rainfall events dominate.

Table 1 also summarizes the effect of deforestation on local climate for a variety of surface variables from each experiment. The hydrological cycle is significantly weakened by deforestation, with a reduction in evaporation, rainfall and runoff. Surface runoff is reduced as the decrease in intensity and frequency of rainfall events predominates over an opposing tendency for increased runoff that is the result of a reduction in infiltration capacity. The decrease in available soil moisture occurs as a result of the marked reduction in root depth (from 127.4 cm to 61.9 cm). Pasture reflects more solar radiation than does forest, which is a very efficient absorber and scatterer of short-wavelength radiation. Consequently, the net energy absorbed by the surface was diminished, with the mean albedo increased from 0.136 to 0.188. By itself, a reduction in net absorption of radiation at the surface would result in a temperature decrease but this is offset by a reduction in evaporative cooling and so there is an overall rise in temperature. The decrease in the latent-heat flux was due to the reduction in roughness (from 0.79 m to 0.04 m) and, at some times of the year, the water availability; this decrease is primarily responsible for the marked increase in the Bowen ratio (defined as the ratio of sensible to latent heat).

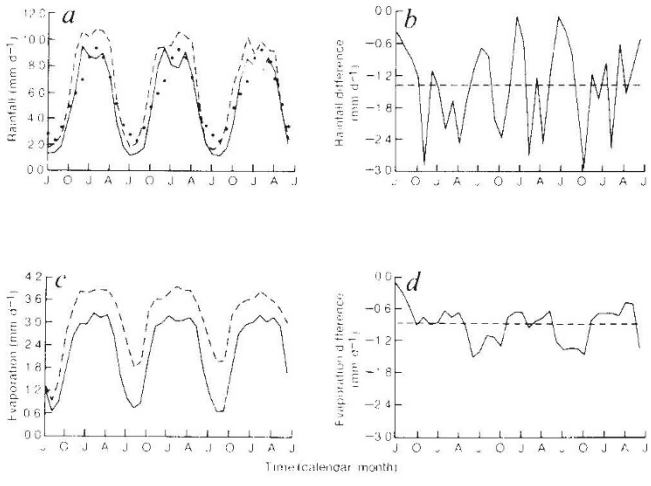

FIG. 2 *a*, Monthly mean precipitation (mm d^{-1}) averaged over the region under consideration for three years starting in July. The broken line represents the control simulation (C), the solid line the deforested simulation (D) and the dots the observed rainfall (O) (ref. 21). *b*, Simulated monthly mean difference (D − C) of precipitation (mm d^{-1}) averaged over the region under consideration for three years starting in July. The broken line represents the mean difference precipitation. *c*, As for *a* but for evaporation (mm d^{-1}). *d*, as for *b* but for evaporation (mm d^{-1}).

Figure 2 depicts the seasonal variation of precipitation and evaporation for the control simulation, the 'deforested' simulation and the difference between the two. There is a consistent decrease in precipitation and evaporation throughout the year although rainfall changes exhibit greater variability. There is also a seasonal variation in the change in evaporation with the maximum differences occurring in the winter and spring when evaporation is controlled by the limited availability of soil moisture.

To gain a better understanding of the physical mechanisms that are operating, two eight-month simulations, using the same initial data as the control and deforested experiments, were carried out to investigate the relative impact that is due to changes to albedo and roughness alone. Table 2 summarizes the differences between some of the surface variables of the control simulation and those of the experiments with increased albedo (from 0.136 to 0.188), decreased roughness (from 0.79 m to 0.04 m), and total deforestation. Precipitation within the Amazon basin originates from two sources—from the recycling of water vapour released during evapotranspiration, and from the moisture flux convergence into this area. The decrease in moisture flux convergence (measured as the difference between precipitation and evaporation) is due mainly to increased albedo although there is some contribution from the change in roughness. Increased albedo reduces the heat source, weakening ascent and boundary-layer convergence[16]. Reduced roughness can also decrease the moisture flux convergence as it weakens the boundary-layer convergence (associated with frictional drag near the surface) into the continental surface-pressure low[17]. Decreased roughness dominates the reduction in evaporation and the associated temperature increase. The forest canopy is wet for most of the year (implying low surface resistance) and so a decrease in evaporation is to be expected as roughness decreases[18]. Increased albedo reduces the available energy for upward turbulent transfer of latent energy. Hence, changes in both albedo and roughness make a major contribution to the overall decreases in precipitation and evaporation in the deforestation experiment.

Our results can be compared with a 13-month simulation carried out by Dickinson and Henderson-Sellers[19]. They incorporated a land surface scheme with a canopy in the National Center for Atmospheric Research Community Climate Model which has a grid resolution of 4.5° × 7.5°. They assumed that all of the Amazon tropical forest in South America was replaced by impoverished grassland. Both experiments show a decrease in evaporation (~16 mm $month^{-1}$ in ref. 19 (from their Fig. 11) compared with 26 mm $month^{-1}$ here) and an increase in surface temperature (with a range of 2.0–5.0 °C over the 13 months in ref. 19 compared with the average of 2.4 °C here). Dickinson

TABLE 2 Summary of the differences in surface variables

Surface Quantity	A − C*	R − C†	D − C‡
Evaporation (E) (mm d^{-1})	−0.20	−0.43	−0.61
Precipitation (P) (mm d^{-1})	−0.75	−0.69	−1.34
$P - E$ (mm d^{-1})	−0.55	−0.26	−0.73
Temperature (°C)	−0.10	2.24	1.98

These results are averaged over eight months.
* A, increased albedo simulation; C, control simulation.
† R, decreased roughness simulation.
‡ D, 'deforested' simulation.

and Henderson-Sellers, however, found no detectable change in rainfall, in contrast to the average decrease of 1.3 mm d^{-1} (20%) shown here.

Our results indicate a stronger impact of deforestation on the local climate than do previous GCM experiments. We note, however, that these results are highly sensitive to the formulations of the model and our ability to make firm predictions based on these results is inhibited by the lack of observations in forested and deforested areas with which to verify these schemes. More ground-based measurements of atmospheric and hydrological processes, together with global data sets of surface vegetation types derived from satellite data, could aid in this development, both as input to the model and to validate and adjust the land surface parameterizations[20]. Nevertheless, our results indicate that deforestation can cause significant local climatic perturbations and further efforts should be made to improve our understanding of the processes involved. □

Received 22 August; accepted 13 October 1989.

1. Dickinson, R. E. (ed.) *The Geophysiology of Amazonia* 3-10 (Wiley, New York, 1987).
2. Fearnside, P. M. in *The Geophysiology of Amazonia* (ed. Dickinson, R. E.) 37-61 (Wiley, New York, 1987).
3. Malingreau, J. P. & Tucker, C. J. *Ambio* **17,** 49-55 (1988).
4. Neto, R. B. *Nature* **339,** 86 (1989).
5. Lavelle, P. in *The Geophysiology of Amazonia* (ed. Dickinson, R. E.) 175-223 (Wiley, New York, 1987).
6. Salati, E., Marques, J. & Molion, L. C. B. *Interciencia* **3,** 200-205 (1978).
7. Salati, E. in *The Geophysiology of Amazonia* (ed. Dickinson, R. E.) 273-296 (Wiley, New York, 1987).
8. Henderson-Sellers, A. in *The Geophysiology of Amazonia* (ed. Dickinson, R. E.) 463-496 (Wiley, New York, 1987).
9. Slingo, A., Wilderspin, R. C. & Smith, R. N. B. *J. geophys. Res.* **94,** 2281-2301 (1989).
10. Smith, R. N. B. *Q. Jl R. met. Soc.* (in the press).
11. Warrilow, D. A. in *Proc. Int. Satellite Land-Surface Climatology Proj.* 159-166 (European Space Agency, 1986).
12. Wilson, M. F. & Henderson-Sellers, A. *J. Clim.* **5,** 119-143 (1985).
13. Warrilow, D. A. & Buckley, E. *Annls Geophys.* **7,** 439-450 (1989).
14. Shuttleworth, W. J. *Proc. R. Soc.* B**233,** 321-346 (1988).
15. Shuttleworth, W. J. & Dickinson, R. E. *Q. Jl R. met. Soc.* **115,** 1177-1179 (1989).
16. Charney, J. G. *Q. Jl R. met. Soc.* **101,** 193-202 (1975).
17. Sud, Y. C., Shukla, J. & Mintz, Y. *J. appl. Met.* **27,** 1036-1054 (1988).
18. Rowntree, P. R. *U.N. Univ. Workshop, Forests, Climate and Hydrology—Regional Impacts* (United Nations University, Tokyo, 1984).
19. Dickinson, R. E. & Henderson-Sellers, A. *Q. Jl R. met. Soc.* **114,** 439-462 (1988).
20. *Int. Satellite Land-Surface Climatology Proj. Report No.* 10 (eds Becker, F., Bolle, H. J. & Rowntree, P. R.) (Free University of Berlin, 1987).
21. Willmott, C. J., Rowe, C. M. & Mintz, Y. *J. Clim.* **5,** 589-606 (1985).
22. Jaeger, L. *Monatskarten Des Niederschlags Fur Die Ganze Erde. Bericht Deutsche Wetterdienst* **18,** no. 139 (1976).
23. *Discharge of Selected Rivers of the World.* Vol. 2 (UNESCO, Paris, 1971).
24. Schutz, C. & Gates, W. L. *Report for Advanced Research Projects Agency; Global Climatic Data for Surface, 800 mb, 400 mb, January* (1971); *July* (1972); *April* (1973); *October* (1974); (Rand, Santa Monica).

ACKNOWLEDGEMENTS. We thank P. R. Rowntree for his guidance in the analysis.

Climate patterns revealed by pollen and oxygen isotope records of a Tyrrhenian sea core

Martine Rossignol-Strick & Nadine Planchais

Laboratoire de Palynologie, URA 327 du CNRS, Université de Montpellier II, Sciences et Techniques du Languedoc, 34095 Montpellier Cedex 2, France

THE analysis of pollen from marine cores has produced continental palaeoclimate records which have been directly correlated with the oxygen isotope record of global ice volume and regional climate[1–3]. Here we tie the palaeoclimate of southern Europe to this global climate signal by reporting continuous pollen and $\delta^{18}O$ records of a well-dated core in the Tyrrhenian Sea for the time span of 55–9 kyr BP. These records show a strong covariation between the marine $\delta^{18}O$ reversed curve and a good terrestrial climate indicator, namely the pollen abundance of deciduous oak from the upland sub-humid Mediterranean forest of southern Italy and Sicily, which seems mainly constrained by moisture variation. The *Artemisia* and grass pollen abundances document the shift between continental semi-desert and oceanic steppe climates. Repetitive successions between 55 and 33 kyr BP of grass, oak, *Artemisia* and *Abies* pollen abundance peaks occur in locked phase with $\delta^{18}O$ depletion events and indicate that regional vegetation cycles closely accompany deglacial pulses of global extent.

The stratigraphy of core KET 8003 (38°49.2′ N, 14°29.5′ E, 1,900 m water depth, 1,030 cm length), is based on the oxygen isotope variation in the foraminifer *Globigerina bulloïdes*, measured at 10-cm intervals[4] (Fig. 1). Tests of calcite formed by marine organisms reflect the fluctuations of ^{18}O in sea water. Because ^{16}O evaporates more readily than ^{18}O, the $^{18}O/^{16}O$ ratio is low in continental ice sheets and high in the glacial ocean. Conversely, during interglacial periods, the oceans are depleted in ^{18}O. The basis of this core lies within the last Interglacial, that is isotope stage 5e at 125 kyr BP. The chronology is based on six interbedded ash layers that have been correlated by their chemical composition with lava flows in southern Italy[4,5] that were dated by ^{14}C and K/Ar analysis to be between 55 and 12 kyr old, and on the initiation of the deglaciation after the last glacial maximum (Termination I), globally seen at 15 kyr BP[6]. Because the sample set for pollen was taken subsequently, it has a 2-cm offset from the isotope set. Pollen has not been recovered below 580 cm.

Southern Italy was also the source area for pollen in core KET 8003: both volcanic ash and pollen are airborne. We have identified 128 pollen taxa and excluded *Pinus* from the pollen sum. The large production and strong resistance of *Pinus* pollen to aerobic bacterial degradation, probably linked to its high sporopollenin content[7], often result in over-representation in marine cores[8]. Here we describe the variation of the pollen percentages of *Quercus*, *Abies*, *Populus*, Poaceae, *Artemisia*, Chenopodiaceae and *Ephedra*. A heavy pollen producer, *Quercus* (oak) is the only deciduous tree whose pollen is continuously present in the core. Oak pollen percentage in core KET 8003 shows no correlation with (1) the pollen sum, (2) total pollen concentration per gram of sediment and *Pinus* pollen abundance. These two observations indicate respectively that the percentage is not an artefact of the analysis procedure nor is it controlled by differential pollen preservation before and during burial on the sea floor.

The $\delta^{18}O$ and oak pollen abundance series of core KET 8003 co-vary in phase with each other. The peaks in oak pollen abundance usually just precede those of $\delta^{18}O$ depletion. This, however, is an artefact of the sampling offset and does not preclude the existence of coincident peaks. The partitioning of the records into two types of intervals, one of $\delta^{18}O$ decrease/oak pollen increase (climate improvement) and the other with the reverse relationship (climate deterioration) yields a high correlation between the two data sets during the former intervals ($r = 0.84$), and a lower one during the latter ($r = 0.55$).

During isotope stage 3, characterized by generally high $\delta^{18}O$ values which denote globally glacial conditions between 69 and 24 kyr BP, there are four closely matched events of $\delta^{18}O$ depletions and oak pollen peaks between 580 and 240 cm which can be seen as short-lived deglacial pulses. Each of the two oldest peaks in oak pollen abundance, dated before 50 kyr BP, is set between two other abundance peaks: an earlier one of Poaceae and a later (and larger) one of *Artemisia*. This repetitive succession amounts to a pattern also seen later, during the first half of the deglaciation after 15 kyr BP. Whereas the abundance of oak pollen decreases above 472 cm, that of *Abies* pollen increases strongly between 450 cm and 400 cm, and *Hedera* and *Ilex* pollen appear sporadically. We suggest a correlation with the peaks of *Abies* pollen seen between 2,200 and 2,045 cm in the record of Lake Monticchio in southern Italy[9]. After 33 kyr BP, *Quercus* and *Artemisia* pollen abundances become minimal and Poaceae is the prevailing herbaceous pollen taxon.

During the glacial maximum (240–190 cm), corresponding to part of isotope stage 2 (24–11 kyr BP), the average abundance of oak pollen is at its lowest. Until mid-stage 2, the dominant